Journal of Sound and Vibration (1997) **207**(2), 151–173

TRANSVERSE VIBRATION OF MULTI MASS LOADED VARIABLE SECTION BEAMS UNDER RANDOM EXCITATION

D. YADAV, S. KAMLE AND S. TALUKDAR

Department of Aerospace Engineering, *Indian Institute of Technology*, *Kanpur* 208016, *India*

(*Received* 15 *July* 1996, *and in final form* 26 *March* 1997)

Dynamic analysis of non-uniform section beams with general end conditions having arbitrary mass and stiffness distributions and proportional viscous damping distribution with several arbitrarily located point mass loadings has been presented for non-stationary random input excitation. Modal analysis has been employed to obtain expressions for second order response statistics after decoupling the system equations. The natural frequencies and mode shape functions for such beams are obtained in closed form as an intermediate step in the outlined approach. Theoretical results for natural frequencies have been compared with experimental evaluations and with data available in the literature. The complete approach is illustrated with an example of a cantilever beam subjected to support excitation.

1. INTRODUCTION

Beams are common structural elements in engineering application. Dynamic behaviour of beams under time dependent loading is important for their performance and design. In most practical applications, beam geometry varies for economic, structural and architectural reasons leading to variable mass, stiffness and damping distributions. Concentrated masses located along the span are also common. Theoretical analysis with beam models presents an economical option compared to numerical techniques. However, the governing differential equation of motion of such beams has space dependent coefficients and imposes complexities in obtaining the general solution. The solution of these equations for general end conditions has been obtained in closed form only for specific cases. The general problem has been solved only by numerical techniques which are computationally intensive.

Analytical solutions for undamped natural frequencies and mode shapes have been obtained in terms of Bessel function and hypergeometric series for a class of tapered beams [1–5]. Frobenius's method has been applied to find eigenparameters for undamped beams of specific taper [6, 7]. Recently, Abrate [8] has shown that for non-uniform beams with some restricted taper and end conditions, the differential equation of motion can be transformed into the equation of motion of a uniform beam. The two beams then have the same eigenvalues. Analytical solutions for vibration frequencies of uniform beams with single or several point masses and simple boundary conditions have been obtained [9–13].

Non-uniform section beam vibration problems have been attempted by various approximate and numerical techniques such as direct numerical integration, Galerkin,

0022–460X/97/420151 + 23 $25.00/0/sv971071

Rayleigh–Ritz, finite elements, boundary element and differential quadrature methods [14–19]. These techniques need intensive computations for accurate results.

Forced vibration of uniform cantilever beams due to deterministic excitation has been analysed with one or no concentrated mass loadings [20–22]. Approximate techniques have been used to study the deterministic forced vibrational response of non-uniform beam with simple support conditions [23, 24].

Tapered and untapered beam flexural vibrations have been studied for stationary random loading using approximate mode superposition techniques [25–28]. Second order response statistics of non-uniform flexible structures have been attempted after discretization to lumped masses under non-stationary uniformly modulated processes [29, 30].

Closed form analysis for response of arbitrary non-uniform beams carrying arbitrarily located concentrated masses under random excitation has not appeared in the literature. The present paper introduces an analytical approach for evaluation of response statistics of non-uniform section beam carrying concentrated masses at arbitrary locations. The approach can accommodate general variations of the taper shape and distribution of mass and stiffness while the distributed viscous damping is proportional to the mass. The natural frequencies and mode shape functions, also very important in themselves, are obtained in closed form as an intermediate step and have been utilized to discretize the equation of motion of the beam in terms of its generalized co-ordinates. The response statistics have been obtained after decoupling the equations of motion. The approach effects significant saving in computational effort. The dynamic excitation process has been considered as non-stationary and is described by the generalized power spectral density (PSD) function. Experiments have been conducted to determine the natural frequencies of tapered beams with concentrated masses for clamped–free, clamped–clamped and pinned–pinned support conditions. Theoretical results for natural frequencies have been generated for beams with different tapers, concentrated mass loadings and end conditions. These have been compared with the experimental results and with those available in literature. Response statistics have been presented for mass loaded cantilever beams with two types of taper.

2. PROBLEM FORMULATION

2.1. EQUATION OF MOTION

A beam subject to dynamic load $f(s, t)$ is shown in Figure 1. The governing equation of motion for the transverse vibration of the beam can be written as [31]

$$\frac{\partial^2}{\partial s^2}\left[EI(s)\frac{\partial^2 w}{\partial s^2}\right] + m(s)\frac{\partial^2 w}{\partial t^2} + \sum_{k=1}^{p} M_k \frac{\partial^2 w}{\partial t^2}\,\delta(s - s_k) + c(s)\frac{\partial w}{\partial t} = f(s, t), \tag{1}$$

where $w(s, t)$ is the transverse displacement of the beam at station s from the origin at instant t and measured positive upwards from the elastic axis, E is the Young's modulus of elasticity of beam material; $m(s)$ is the mass per unit length of the beam; $c(s)$ is the distributed viscous damping per unit length; M_k $(k = 1, 2, \ldots, p)$ are the concentrated masses at stations s_k; $\delta(\cdot)$ is the Dirac delta function.

Mass per unit length of the beam can be expressed as

$$m(s) = \rho A(s), \tag{2}$$

in which ρ is the density of the beam material and $A(s)$ is the cross-sectional area.

2.2. EXTERNAL EXCITATION

The external excitation $f(s, t)$ on the beam is assumed to be random in time parameter but deterministic in space. It may, in general, be non-stationary in nature. The excitation may be represented as

$$f(s, t) = f_m(s, t) + f_R(s, t) \tag{3}$$

where $f_m(s, t)$ is the mean process and $f_R(s, t)$ is a zero mean random process. The random part may be represented in Stieltjes form [32] as

$$f_R(s, t) = \int_{-\infty}^{\infty} \mathrm{d}S_{f_R}(s, \omega) \exp(\mathrm{j}\omega t), \tag{4}$$

where $\mathrm{d}S_{f_R}(s, \omega)$ possesses the following property

$$E[\mathrm{d}S_{f_R}(s, \omega)] = \mu_{f_R}(s, \omega)\,\mathrm{d}\omega = 0,$$

$$E[|\,\mathrm{d}S_{f_R}(s_1, \omega_1)\,\mathrm{d}S^*_{f_R}(s_2, \omega_2)\,|] = \Phi_{f_R f_R}(s_1, \omega_1; s_2, \omega_2)\,\mathrm{d}\omega_1\,\mathrm{d}\omega_2, \tag{5}$$

where μ_{f_R} is the mean and $\Phi_{f_R f_R}$ is the generalized PSD function of the random process f_R.

2.3. NATURAL FREQUENCIES AND MODE SHAPES

Equation (1) can be rewritten as

$$\frac{\partial^2}{\partial s^2}\left[EI(s)\frac{\partial^2 w}{\partial s^2}\right] + m(s)\frac{\partial^2 w}{\partial t^2} + c(s)\frac{\partial w}{\partial t} = -\sum_{k=1}^{p} M_k \frac{\partial^2 w}{\partial t^2}\,\delta(s - s_k) + f(s, t). \tag{6}$$

Equation (6) is equivalent to a forced vibrating system with inertial reaction of the concentrated masses contributing to the externally applied load. Let the homogeneous solution be of the form

$$w(s, t) = W(s) \exp(\zeta + \mathrm{j}\Omega)t, \tag{7}$$

where $W(s)$ is the mode shape function, Ω is the damped natural frequency, ζ is a factor related to the damping and j is the imaginary unit equal to $\sqrt{-1}$. Substitution of this in

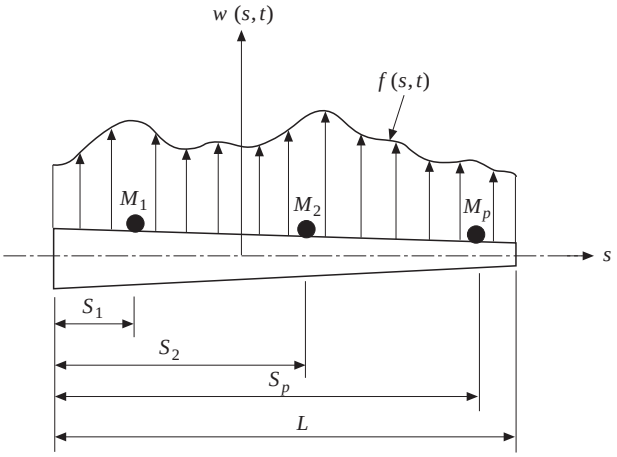

Figure 1. Beam model.

the homogeneous part of equation (6) yields

$$\frac{\mathrm{d}^2}{\mathrm{d}s^2}\left[EI(s)\frac{\mathrm{d}^2W}{\mathrm{d}s^2}\right] + m(s)(\zeta + \mathrm{j}\Omega)^2 W(s) + c(s)(\zeta + \mathrm{j}\Omega)W(s) = 0. \tag{8}$$

Let the variable moment of inertia, cross-sectional area and damping be expressed by the following power series

$$I(s) = I(0)f_1(s); \qquad f_1(s) = \sum_{i=0}^{\infty} p_i s^i, \qquad c(s) = c(0)f_2(s), \qquad A(s) = A(0)f_2(s)$$

and

$$m(s) = \rho A(0) f_2(s); \qquad f_2(s) = \sum_{i=0}^{\infty} q_i s^i. \tag{9}$$

where $I(0)$, $A(0)$, $c(0)$ are the moment of inertia, cross-sectional area and damping at the reference section. The coefficients of the series $f_1(s)$ and $f_2(s)$ can be matched to fit any desired variation of these properties. The implication of equation (9) is that any form of variation in stiffness and mass distributions is accommodated by the method. However, the distribution of the viscous damping has to be proportional to the mass.

Substitution of equation (9) in equation (8) yields

$$f_1(s)\frac{\mathrm{d}^4W}{\mathrm{d}s^4} + 2\frac{\mathrm{d}f_1}{\mathrm{d}s}\frac{\mathrm{d}^3W}{\mathrm{d}s^3} + \frac{\mathrm{d}^2f_1}{\mathrm{d}s^2}\frac{\mathrm{d}^2W}{\mathrm{d}s^2} - \lambda^4 f_2(s)W(s) = 0, \tag{10}$$

where

$$\lambda^4 = \frac{\rho A(0)}{EI(0)}[(\Omega^2 - \zeta^2 - D\zeta) - \mathrm{j}\Omega(2\zeta + D)], \tag{11}$$

with $D = c(0)/\rho A(0)$.

Introducing a new independent variable $x = \lambda s$ in equation (10) transforms it to

$$\overline{f}_1(x)\frac{\mathrm{d}^4W}{\mathrm{d}x^4} + 2\frac{\mathrm{d}\overline{f}_1}{\mathrm{d}x}\frac{\mathrm{d}^3W}{\mathrm{d}x^3} + \frac{\mathrm{d}^2\overline{f}_1}{\mathrm{d}x^2}\frac{\mathrm{d}^2W}{\mathrm{d}x^2} - \overline{f}_2(x)W = 0, \tag{12}$$

where

$$\overline{f}_1(x) = \sum_{k=0}^{\infty} \bar{p}_k x^k, \qquad \overline{f}_2(x) = \sum_{k=0}^{\infty} \bar{q}_k x^k, \tag{13}$$

with

$$\bar{p}_k = p_k/\lambda^k \quad \text{and} \quad \bar{q}_k = q_k/\lambda^k. \tag{14}$$

A series solution for $W(x)$ in equation (12) is assumed

$$W(x) = \sum_{i=0}^{\infty} \bar{c}_i x^i. \tag{15}$$

Using W and its derivatives along with equation (13) in equation (12) and following the product rule of two series [33], one has

$$\sum_{n=0}^{\infty} (P_n + Q_n + R_n - S_n)x^n = 0, \tag{16}$$

where

$$P_n = \sum_{k=0}^{n} (n-k+1)(n-k+2)(n-k+3)(n-k+4)\bar{p}_k \bar{c}_{n-k+4}, \tag{17}$$

$$Q_n = \sum_{k=0}^{n} 2(k+1)(n-k+1)(n-k+2)(n-k+3)\bar{p}_{k+1} \bar{c}_{n-k+3}, \tag{18}$$

$$R_n = \sum_{k=0}^{n} (k+1)(k+2)(n-k+1)(n-k+2)\bar{p}_{k+2} \bar{c}_{n-k+2}, \tag{19}$$

$$S_n = \sum_{k=0}^{n} \bar{q}_k \bar{c}_{n-k}. \tag{20}$$

Since equation (16) must be satisfied for every value of x, it implies that the coefficient of each power of x must vanish. Thus one has

$$\bar{c}_{n+4} = \frac{1}{(n+1)(n+2)(n+3)(n+4)\bar{p}_0}\left[\sum_{k=0}^{n} \{\bar{q}_k \bar{c}_{n-k} - (n-k+1)(n-k+2)(k+1) \times (2(n-k+3)\bar{p}_{k+1}\bar{c}_{n-k+3} + (k+2)\bar{p}_{k+2}\bar{c}_{n-k+2})\} - \sum_{k=1}^{n} (n-k+1)(n-k+2)(n-k+3)(n-k+4)\bar{p}_k \bar{c}_{n-k+4}\right], \quad n = 0, 1, 2, \ldots . \tag{21}$$

Equation (21) gives a recurrence relationship which can be used to determine the unknown coefficients of the series W except the first four coefficients $\bar{c}_0$, $\bar{c}_1$, $\bar{c}_2$, and $\bar{c}_3$. These four have to be determined with the help of the beam boundary conditions. All other coefficients $\bar{c}_i$ ($i = 4, 5, \ldots$) can be expressed in terms of the first four basic coefficients. Thus

$$\bar{c}_i = \sum_{k=0}^{3} L_{ik} \bar{c}_k, \qquad i = 4, 5, \ldots, \tag{22}$$

where $L_{ik} = f_i(p_1, p_2, \ldots, q_1, q_2, \ldots, \lambda)$.

Expressing all coefficients of the series in terms of the first four coefficients, it is now possible to write the mode shape function as

$$W(s) = \bar{c}_0 + \bar{c}_1 \lambda s + \bar{c}_2 \lambda^2 s^2 + \bar{c}_3 \lambda^3 s^3 + \sum_{i=4}^{\infty} \sum_{k=0}^{3} L_{ik} \bar{c}_k \lambda^i s^i, \tag{23}$$

and in a more compact form,

$$W(s) = \sum_{i=0}^{3} g_i(p_1, p_2, \ldots, q_1, q_2, \ldots, \lambda, s) c_i. \tag{24}$$

The application of appropriate boundary conditions of the beam in equation (24) results in the eigenvalue problem

$$\mathbf{Bc} = \mathbf{0} \tag{25}$$

where the elements of the matrix **B** contain W and its derivatives evaluated at beam boundaries. The elements of the vector **c** contain unknown coefficients $\bar{c}_0$, $\bar{c}_1$, $\bar{c}_2$ and $\bar{c}_3$. The roots of the characteristic equation give multiple values of λ, which upon substitution in equation (24), yields the vector **c**. This can now be utilized for evaluation of the mode shape function W. The damped natural frequencies are obtained from equation (11).

2.4. DECOUPLING OF THE SYSTEM EQUATION

By adopting the mode superposition principle, it is possible to express the beam response as

$$w(s, t) = \sum_{i=1}^{\infty} W_i(s) q_i(t), \tag{26}$$

where q_i are the normal co-ordinates.

Substituting equation (26) in equation (6), multiplying the resulting equation by W_k, integrating in the beam domain and invoking the orthogonality condition of normal modes [31], one has

$$\left[\ddot{q}_i(t) + \frac{1}{M_{gi}} \sum_{l=1}^{p} M_l W_i(s_l) \sum_{k=1}^{\infty} W_k(s) \ddot{q}_k(t)\right] + D\dot{q}_i(t)$$
$$\times [(\Omega_i^2 - \zeta_i^2 - D\zeta_i) - \mathrm{j}\Omega_i(2\zeta + D)] q_i(t) = F_i(t), \tag{27}$$

where M_{gi} is the generalized mass and F_j is the generalized force associated with the ith mode. These are given as,

$$M_{gi} = \int_L m(s) W_i^2(s)\, \mathrm{d}s, \qquad F_i(t) = \frac{1}{M_{gi}} \int_L f(s, t) W_i(s)\, \mathrm{d}s. \tag{28}$$

Equation (27) shows inertia coupling in the presence of concentrated masses. The number of normal co-ordinates are theoretically infinite. However, assuming that the higher order modes do not contribute as significantly as the lower modes, the number of significant terms in the infinite summation can be truncated to a finite size. Let n be the number of significant modes. Then n number of coupled equations (27) can be expressed in matrix notation

$$\mathbf{M}\ddot{\mathbf{q}}(t) + \mathbf{C}\dot{\mathbf{q}}(t) + \mathbf{K}\mathbf{q}(t) = \mathbf{F}(t), \tag{29}$$

where **M**, **C**, **K** are system mass, damping and stiffness matrices respectively. Equation (29) can be expanded to $2n$ coupled first order equations as

$$\dot{\mathbf{p}} + \mathbf{G}\mathbf{p} = \mathbf{P}, \tag{30}$$

where

$$\mathbf{p} = \left\{\begin{array}{c} \dot{\mathbf{q}} \\ \hline \mathbf{q} \end{array}\right\}, \qquad \mathbf{P} = \left\{\begin{array}{c} \mathbf{M}^{-1}\mathbf{F} \\ \hline \mathbf{0} \end{array}\right\} \quad \text{and} \quad \mathbf{G} = \left\{\begin{array}{c|c} \mathbf{M}^{-1}\mathbf{C} & \mathbf{M}^{-1}\mathbf{K} \\ \hline -\mathbf{I} & -\mathbf{0} \end{array}\right\}. \tag{31}$$

I is the identity matrix and **0** is the null vector/matrix. Let the eigenvalues of the matrix **G** be $\alpha_1, \alpha_2, \ldots, \alpha_{2n}$ and the corresponding eigenvectors $\{\mathbf{u}\}^1, \{\mathbf{u}\}^2, \ldots, \{\mathbf{u}\}^{2n}$. The imaginary part of the eigenvalues gives the damped natural frequencies of the variable section point mass loaded beam system.

The modal matrix is defined as

$$\mathbf{U} = [\{\mathbf{u}\}^1\{\mathbf{u}\}^2 \ldots \{\mathbf{u}\}^{2n}]. \tag{32}$$

The eigenvalues are assumed to be distinct. Thus one has [34]

$$\mathbf{U}^{-1}\mathbf{G}\mathbf{U} = \text{diagonal}\,[\alpha_1, \alpha_2, \ldots, \alpha_{2n}]. \tag{33}$$

Using a linear transformation

$$\mathbf{p} = \mathbf{U}\mathbf{v} \tag{34}$$

and condition (33) in equations (30), these can be decoupled as

$$\dot{v}_i(t) + \alpha_i v_i(t) = R_i(t), \qquad i = 1, 2, \ldots, 2n, \tag{35}$$

where

$$R_i = \sum_{i=1}^{n} \bar{u}_{ir} \sum_{k=1}^{n} \bar{m}_{rk} F_k \tag{36}$$

and u_{ir} denote elements in the inverse of the matrix **U** and $\bar{m}_{rk}$ the elements in the inverse of the matrix **M**.

2.5. BEAM RESPONSE TO EXTERNAL EXCITATION

2.5.1. *General solution*

The general solution of equation (35) in Stieltjes integral form may be expressed as

$$v_i(t) = X_{oi} \exp(-\alpha_i t) + \int_{-\infty}^{\infty} H_i(\omega, t)\, \mathrm{d}S(R_i(\omega)), \tag{37}$$

where X_{oi} are constants of integration to be determined from the initial conditions. $H_i(\omega, t)$ is the transient frequency response function given by [34]

$$H_i(\omega, t) = \frac{1}{\mathrm{j}\omega + \alpha_i}\,[\exp(\mathrm{j}\omega t) - \exp\{-\alpha_i(t - t_o)\}]. \tag{38}$$

It can be seen that as $t_o \to -\infty$, for the positive real part of α_i, which is the characteristics of a stable system, $H_i(\omega, t)$ approaches a limiting value $(1/\mathrm{j}\omega + \alpha_i)\exp(\mathrm{j}\omega t)$.

Using equations (34) and (36) in equation (37), the response in generalized normal co-ordinates may be expressed as

$$q_m(t) = \sum_{i=1}^{2n} u_{m+n,i}\, X_{oi} \exp(-\alpha_i t) + \sum_{i=1}^{2n} u_{m+n,i} \sum_{r=1}^{n} \bar{u}_{ir} \sum_{k=1}^{n} \bar{m}_{rk}$$

$$\times \int_{-\infty}^{\infty} H_i(\omega, t)\, \mathrm{d}S(R_i(\omega)); \qquad m = 1, 2, \ldots, n. \tag{39}$$

2.5.2. *Response statistics*

The mean and covariance for the generalized normal co-ordinates are given by

$$\mu_{q_m}(t) = E[q_m(t)], \tag{40}$$

$$K_{q_i q_k}(t_1, t_2) = E[\{q_i(t_1) - \mu_{q_i}(t_1)\}\{q_k(t_2) - \mu_{q_k}(t_2)\}^*]. \tag{41}$$

Substituting equation (39) in equation (40), one has

$$\mu_{q_m}(t) = \sum_{i=1}^{2n} u_{m+n,i} X_{oi} \exp(-\alpha_i t) + \sum_{i=1}^{n} u_{m+n,i} \sum_{r=1}^{n} u_{ir} \sum_{k=1}^{n} m_{rk} I_{ik}(t), \qquad m = 1, 2, \ldots, n, \tag{42}$$

where

$$I_{ik}(t) = \int_{-\infty}^{\infty} H_i(\omega, t) E[\mathrm{d}S_{F_k}(\omega)]. \tag{43}$$

Using the expression for the kth generalized force F_k from equation (28), the above integral becomes

$$I_{ik}(t) = \frac{1}{M_{gk}} \int_{-\infty}^{\infty} \int_{0}^{L} H_i(\omega, t) E[\mathrm{d}S_f(s, \omega)] W_k(s)\, \mathrm{d}s$$

$$= \frac{1}{M_{gk}} \int_{-\infty}^{\infty} \int_{0}^{L} H_i(\omega, t) \mu_{f_m}^*(s, \omega) W_k(s)\, \mathrm{d}s\, \mathrm{d}\omega, \tag{44}$$

where $\mu_{f_m}^*$ is the Fourier transform of the mean excitation f_m and is defined by

$$\mu_{f_m}^*(s, \omega) = \frac{1}{2\pi} \int_{-\infty}^{\infty} f_m(s, \tau) \exp(-\mathrm{j}\omega\tau)\, \mathrm{d}\tau. \tag{45}$$

Substitution of equations (38) and (45) in equation (44) yields

$$I_{ik}(t) = \frac{1}{M_{gk}} \int_{-\infty}^{\infty} \int_{0}^{L} f_m(s, \tau) \left[\frac{1}{2\pi} \int_{-\infty}^{\infty} \frac{1}{\mathrm{j}\omega + \alpha_i} \exp(\mathrm{j}\omega(t - \tau))\, \mathrm{d}\omega \right] W_k(s)\, \mathrm{d}s\, \mathrm{d}\tau.$$

After evaluation of the inner integral over ω, I_{ik} takes the form

$$I_{ik}(t) = \frac{1}{M_{gk}} \int_{-\infty}^{\infty} \int_{0}^{L} f_m(s, \tau) W_k(s) \exp(-\alpha_i(t - \tau))\, \mathrm{d}s\, \mathrm{d}\tau. \tag{46}$$

Considering the fact that the excitation is not present for $\tau < 0$ and is available only up to $\tau \leqslant t$, lower and upper limits of the time integral may be changed to 0 and t.

Using equations (39) and (42) in equation (41), the expression for the covariance response can be put as

$$K_{q_i q_k}(t_1, t_2) = \sum_{l=1}^{2n} \sum_{r=1}^{n} \sum_{p=1}^{2n} \sum_{a=1}^{n} \sum_{b=1}^{n} \sum_{w=1}^{n} u_{i+n,l} \bar{u}_{lr} \bar{m}_{ra} u_{k+n,p} \bar{u}_{pb} \bar{m}_{bw} \{I_{a,b}(t_1, t_2) - I_{la}(t_1) I_{pb}(t_2)\},$$

$$i, k = 1, 2, \ldots, n, \tag{47}$$

where

$$I_{a,b}(t_1, t_2) = \int_{-\infty}^{\infty} \int_{-\infty}^{\infty} H_l(\omega_1, t_1) H_p^*(\omega_2, t_2) E[\mathrm{d}S_{F_a}(\omega_1)\, \mathrm{d}S_{F_b}^*(\omega_2)]. \tag{48}$$

Substituting the expression for the generalized forces F_a and F_b from equation (28), the above integral can be expressed as

$$I_{a,b}(t_1, t_2) = \frac{1}{M_{ga}} \frac{1}{M_{gb}} \int_{-\infty}^{\infty} \int_{-\infty}^{\infty} \int_0^L \int_0^L H_l(\omega_1, t_1) H_p^*(\omega_2, t_2)$$
$$\times \Phi_{f_R f_R}(s_1, \omega_1; s_2, \omega_2) W_a(s_1) W_b(s_2)\, \mathrm{d}s_1\, \mathrm{d}s_2\, \mathrm{d}\omega_1\, \mathrm{d}\omega_2. \tag{49}$$

Equations (42) and (47) give expressions for the mean and covariance of the generalized normal co-ordinates. These can be utilized to obtain the response characteristics of the beam once the two basic integrals I_{ik} and $I_{a,b}$ are evaluated. These integrals can be obtained if the characteristics of the input process is known.

2.5.3. *Example of cantilever with support excitation*

In order to illustrate the approach for response statistics evaluation, an example of a cantilever beam with concentrated mass loadings is taken in which dynamic loading is induced due to its support excitation. Let $z(t)$ be the translatory motion of the support, hence

$$f(s, t) = -\{m(s)\ddot{z}(t) + c(s)\dot{z}(t)\}, \tag{50}$$

where the base displacement $z(t)$ can be written as

$$z(t) = z_m(t) + z_R(t), \tag{51}$$

with z_m and z_R being the mean and zero random parts respectively of the process $z(t)$.

Using equation (51), the mean and random part of the exciting force can be expressed as

$$f_m(s, t) = -\{m(s)\ddot{z}_m(t) + c(s)\dot{z}_m(t)\}, \tag{52}$$

$$f_R(s, t) = -\{m(s)\ddot{z}_R(t) + c(s)\dot{z}_R(t)\}. \tag{53}$$

Substitution of equation (52) in equation (46), yields

$$I_{ik}(t) = \int_{-\infty}^{\infty} \{A_k \ddot{z}_m(\tau) + B_k \dot{z}_m(\tau)\} \exp(-\alpha_i(t - \tau))\, \mathrm{d}\tau, \tag{54}$$

where

$$A_k = -\frac{1}{M_{gk}} \int_0^L m(s) W_k(s)\, \mathrm{d}s, \qquad B_k = -\frac{1}{M_{gk}} \int_0^L c(s) W_k(s)\, \mathrm{d}s. \tag{55}$$

Further the PSD of the excitation can be written as

$$\phi_{f_R f_R}(s_1, \omega_1; s_2, \omega_2) = [m(s_1)m(s_2)\omega_1^2\omega_2^2 + \mathrm{j}\{m(s_2)c(s_1)\omega_1\omega_2^2 - m(s_1)c(s_2)\omega_1^2\omega_2\}$$
$$+ c(s_1)c(s_2)\omega_1\omega_2] \Phi_{z_R z_R}(\omega_1, \omega_2). \tag{56}$$

Substituting equation (56) in equation (49) and using equation (55), the integral $I_{a,b}$ becomes

$$I_{a,b}(t_1, t_2) = \int_{-\infty}^{\infty} \int_{-\infty}^{\infty} H_l(\omega_1, t_1) H_p^*(\omega_2, t_2) \{A_a A_b \omega_1^2 \omega_2^2 + \mathrm{j}(\omega_1^2 \omega_2 A_b B_a - \omega_2^2 \omega_1 A_a B_b) + B_a B_b \omega_1 \omega_2\} \Phi_{z_R z_R}(\omega_1, \omega_2)\, \mathrm{d}\omega_1\, \mathrm{d}\omega_2. \tag{57}$$

It is seen from equations (54) and (57) that evaluation of the integrals I_{ik} and $I_{a,b}$ need the description of z_m and $\phi_{z_R z_R}$.

Any suitable deterministic function can be chosen to represent the mean z_m. In the present study it is assumed as a sinusoidal function of amplitude z_0 and frequency ω_0 as a generic term in a Fourier series expansion. Thus z_m is

$$z_m(t) = z_0 \sin \omega_0 t. \tag{58}$$

It is known that the characteristics of the excitation process depends on the source of its origin. Standard forms of PSD are available in the literature for most known types of excitations. The following PSD [34] has been taken for the base excitation, assumed stationary, in this illustrative example

$$\Phi_{z_R z_R}(\omega) = \sigma^2 \exp(-\omega^2/4\beta_1^2)/2\sqrt{\pi}\beta_1, \tag{59}$$

where σ is the standard deviation of z_R and β_1 is a correlation constant.

As the random process $z_R(t)$ is stationary, one can write

$$\Phi_{z_R z_R}(\omega_1, \omega_2) = \Phi_{z_R z_R}(\omega_1)\delta(\omega_1 - \omega_2). \tag{60}$$

Substituting equation (58) in equation (54), the integral I_{ik} is evaluated as

$$I_{ik}(t) = \frac{z_0 \omega_0^2}{\alpha_i^2 + \omega_0^2} \left[\frac{B_k}{\omega_0} \{\alpha_i \cos \omega_0 t + \omega_0 \sin \omega_0 t - \alpha_i \exp(-\alpha_i t)\} - A_k \{\alpha_i \sin \omega_0 t - \omega_0 \cos \omega_0 t + \omega_0 \exp(-\alpha_i t)\} \right]. \tag{61}$$

Using equations (59) and (60) in equation (57) and evaluating the integral in the complex domain with the help of Cauchy's Residue theorem, one has

$$I_{a,b}(t_1, t_2) = (\sqrt{\pi}\sigma^2/\beta_1)\{\exp(-\alpha_l |t_1 - t_2|) - \exp(-\alpha_l t_1 - \alpha_p t_2)\} \times \exp\{\alpha_l^2/4\beta_1\}\{(A_a A_b \alpha_l^4 + (A_b B_a - B_b A_a)\alpha_l^3 - B_a B_b \alpha_l^2)/(\alpha_l + \alpha_p)\}. \tag{62}$$

Utilizing equations (61) in equation (42), the mean displacement μ_{q_m} $(m = 1, 2, \ldots, n)$ can be obtained. The mean velocity response $\mu_{\dot{q}_m}$ can be found by substituting u_m for u_{m+n} in the expression for μ_{q_m}. The mean acceleration is determined by differentiating $\mu_{\dot{q}_m}$ with time.

Substitution of equations (62) and (61) in equation (47) yields the covariance of the displacement. The velocity covariance $K_{\dot{q}_i \dot{q}_k}(t_1, t_2)$ is known by substituting u_{il} and u_{kp} for $u_{i+n,l}$ and $u_{k+n,p}$ respectively in the expression for $K_{q_i q_k}(t_1, t_2)$. The covariance of acceleration is determined by differentiating the covariance of velocity successively with respect to t_1 and t_2.

TABLE 1

Non-dimensional natural frequency $(\Omega^2 m_0 L^4/EI_0)^{1/2}$ *of linearly tapered beams with no concentrated mass loadings*

End Cond.	Taper t_b, t_h	Result Source	Mode Sequence 1	2	3	4	5
Cl–Fr	0·2, 1·0	*	5·3973	25·6555	65·7473	125·2584	204·3782
		[5]	5·3969	25·656	–	–	–
		[6]	5·3976	25·6558	65·7470	–	–
		[16]	5·3976	25·6560	65·7470	125·2600	204·5500
	1·0, 0·2	*	4·2920	15·7425	36·8848	68·1160	109·9079
		[5]	4·2926	15·7420	–	–	–
		[16]	4·2925	15·743	36·886	68·144	110·06
	0·2, 0·2	*	6·1965	18·3852	39·8335	71·2413	112·8328
		[5]	6·1972	18·384	–	–	–
		[16]	6·1964	18·386	39·8370	71·2880	113·3300
Fr–Cl	0·2, 1·0	*	2·1709	18·9589	58·5574	117·5956	196·5318
		[6]	2·1709	18·9589	58·5574	–	–
Cl–Cl	0·2, 1·0	*	21·4707	60·3316	119·3342	198·1076	295·2434
		[6]	21·4707	60·3321	119·3396	–	–
	1·0, 1·2	*	24·5634	67·7044	132·7371	219·2361	324·8328
		[8]	24·5634	67·7048	132·7240	–	–
Cl–Pn	0·2, 1·0	*	16·5075	51·0248	105·4035	179·0118	272·0306
		[6]	16·5074	51·0250	105·4009	–	–
	1·0, 1·2	*	16·5029	54·4611	114·0600	195·1918	296·6478
		[8]	16·5029	54·4614	114·0516	–	–
Pn–Cl	0·2, 1·0	*	13·4846	47·7671	101·8402	175·7147	268·8754
		[6]	13·4845	47·7672	101·8389	–	–
Pn–Pn	0·2, 1·0	*	9·6722	39·5851	89·0714	158·2421	246·7976
		[6]	9·6721	39·5851	89·0704	–	–
	1·0, 1·2	*	10·8267	43·3565	97·5357	173·3681	271·4061
		[16]	10·8270	43·357	97·535	173·38	271·41

Note: * represents the results from the present work.

3. RESULTS AND DISCUSSIONS

The analysis aims at evaluating the response statistics for mass loaded variable section beams. Remembering the importance of the natural frequencies and mode shapes in understanding the behaviour and performance of the structures, the results are presented in two sections—(a) beam natural frequencies and mode shapes, and (b) response statistics.

3.1. BEAM NATURAL FREQUENCIES AND MODE SHAPES

Theoretical results have been obtained with the present approach for natural frequencies and mode shapes for different end conditions of beams with various tapers and point mass loadings. Some of these results are compared with results available in the literature and obtained experimentally.

3.1.1. *Comparison with results available in literature*

The analytical results from the present approach have been compared with published results and are presented in Tables 1, 2 and 3. The natural frequency is

TABLE 2

Non-dimensional natural frequency $(\Omega^2 m_0 L^4/EI_0)^{1/2}$ *of linearly tapered cantilevered beams with concentrated mass loadings*

Taper t_b, t_h	Result Source	Mode Sequence 1	2	3	4	5
(a) Single concentrated mass $m_r = 0{\cdot}5$, $s_r = 0{\cdot}3$						
1·0, 1·0	*	3·4513	17·4415	47·3072	113·8837	196·6725
	[16]	3·4512	17·430	47·302	113·83	196·35
	$m_r = 0{\cdot}5$, $s_r = 1{\cdot}0$					
	*	2·0156	16·9036	51·7071	106·1008	180·2362
	[16]	2·0163	16·901	51·701	106·06	180·18
	[20]	2·0163	16·901	51·701	106·06	180·12
(b) Three equal concentrated masses $m_r = 0{\cdot}01$; $s_r = 1/3,\ 2/3,\ 1{\cdot}0$						
	*	3·4256	21·3949	59·4744	118·5629	194·3881
	[13]	3·4262	21·3943	59·4734	118·5838	194·4162
	$m_r = 0{\cdot}1$; $s_r = 1/3,\ 2/3,\ 1{\cdot}0$					
	*	2·8406	17·5515	47·7382	109·3044	171·7031
	[13]	2·8406	17·5502	47·7528	109·2080	171·6661
	$m_r = 0{\cdot}2$; $s_r = 1/3,\ 2/3,\ 1{\cdot}0$					
	*	2·4460	15·1708	41·1835	105·3713	162·1602
	[13]	2·4460	15·1688	41·1555	105·3552	162·1501

Note: * represents the results from the present work.

non-dimensionalized to frequency number as $(\Omega^2 m_0 L^4/EI_0)^{1/2}$, where m_0 and I_0 refer to the $s = 0$ end. The larger end is mentioned first in describing the beam end conditions. The ratios of the end widths $b(L)/b(0)$ and end heights $h(L)/h(0)$ are termed as taper ratios and denoted as t_b and t_h respectively. The ratio of the concentrated mass to the beam mass is denoted by m_r and concentrated mass location as a fraction of the beam length is denoted by s_r.

The first two tables are for linearly tapered undamped beams. Table 1 shows the comparison of frequency numbers of beams with no concentrated mass loading and various end conditions. Table 2 is for beams with one or more concentrated masses. Published results are shown for various references indicated in the tables. Frequency

TABLE 3

Non-dimensional frequency parameter $(\Omega^2 m_0 L^4/EI_0)^{1/2}$ *of parabolically tapered beams*

End Cond.	Taper t_b, t_h	Result Source	Mode Sequence 1	2	3	4	5
Cl–Fr	0·2, 1·0	*	5·3069	25·4162	65·2273	125·0085	204·1635
		[16]	5·3301	25·4350	65·4870	125·0300	204·4500
	1·0, 0·2	*	3·1658	12·0357	28·3321	53·1875	86·0057
		[16]	3·1790	12·0850	28·9321	53·5540	86·7310
	0·2, 0·2	*	4·4116	13·8623	30·2585	55·2786	89·1842
		[16]	4·4454	13·9330	30·9930	55·9614	89·6730

Note: * represents the results from the present work.

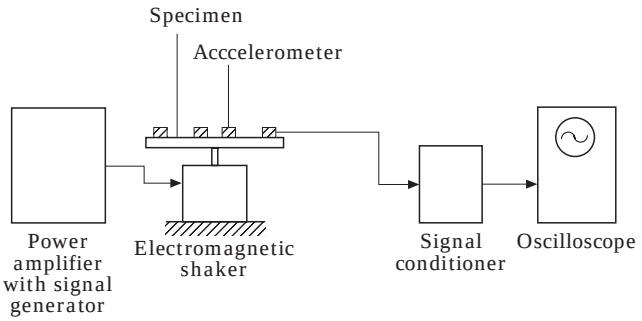

Figure 2. Block diagram of experimental set up.

numbers for parabolically tapered beams are presented in Table 3. Beam sections similar to reference [16] have been selected for this table.

Comparison shows good agreement between the analytical values obtained and published results. The agreement is better for the lower modes, which is as expected.

3.1.2. *Comparison with experimental results*

Experiments have been conducted on variable section beams with three classical support conditions: clamped–free, pinned–pinned and clamped–clamped. A schematic diagram for the experimental set up is shown in Figure 2.

The clamped end condition was simulated by bolting the beam end between two mild steel plates by six bolts of 6 mm diameter. The size of the base plate was 100 mm × 100 mm × 10 mm and was welded to a heavy frame. The cover plate had a size of 100 mm × 100 mm × 6 mm. The pinned end condition was simulated with the help a fixture carrying two shafts vertically above one another. Each shaft was mounted with three sets of ball bearings. The lower shaft was held in position while the upper shaft could be raised or lowered with the help of a screw arrangement. The beam end was accommodated between the upper and the lower ball bearings. The upper shaft was lowered to just make bearing contact with the top of the beam surface. This allowed freedom of rotation to the beam end with no vertical displacement. The arrangement was housed in a rigid frame constructed with 150 mm × 75 mm × 10 mm mild steel channel section.

The beam was excited harmonically by an electromagnetic shaker (capacity 62·5 kg) through a power amplifier. The power amplifier used has a built-in sinusoidal waveform

TABLE 4

Experimental validation of natural frequency ($t_b = 0{\cdot}4$, $t_h = 1{\cdot}0$)

Specimen No.	Support condition	Source of Result	Natural frequencies (Hz) f_1	f_2	f_3
B1	Cl–Fr	Theory	27·62	187·79	444·69
		Experiment	27·00	190·00	451·00
	Pn–Pn	Theory	103·33	325·00	770·00
		Experiment	107·00	337·00	790·00
B2	Cl–Cl	Theory	46·74	130·05	250·18
		Experiment	43·00	125·00	241·00

generator which provides a low harmonic content, variable amplitude, variable frequency, sine wave output. The frequency of the wave can be adjusted from 1 Hz to 20 kHz in seven overlapping ranges. In the experiment, the driving frequency was monitored through the power amplifier and was varied to match the resonant frequency. Accelerometers weighing 0·0296 kg were mounted at planned locations on the beam and were treated as concentrated masses. The output signals from the accelerometers were passed through a signal conditioner and observed in an oscilloscope to identify the event of resonance and the corresponding frequency was recorded. The oscilloscope used has a dual trace plug-in unit having a sensitivity of 0·005 to 2 V/mm.

Two different specimens of aluminum ($\rho = 2744$ kg/m^3, $E = 70$ GPa) beam have been tested. Details of the specimens and their support conditions are:

*Specimen B*1: $L = 0{\cdot}3$ m, $b(0) = 0{\cdot}05$ m, $h(0) = 0{\cdot}00325$ m, $b(L) = 0{\cdot}02$ m. End conditions: clamped–free and pinned–pinned. Concentrated mass: $M_1 = 0{\cdot}0296$ kg, $s_1 = 0{\cdot}15$ m.

*Specimen B*2: $L = 0{\cdot}60$ m, $b(0) = 0{\cdot}1$ m, $h(0) = 0{\cdot}00385$ m, $b(\mathrm{L}) = 0{\cdot}04$ m. End conditions: clamped–clamped; Concentrated masses: $M_1 = M_2 = M_3 = M_4 = 0{\cdot}0296$ kg; concentrated mass locations: $s_1 = 0{\cdot}135$ m, $s_2 = 0{\cdot}295$ m, $s_3 = 0{\cdot}426$ m, $s_4 = 0{\cdot}58$ m.

The experimental values of the first three natural frequencies are given along with the theoretical value in Table 4. These show that the first three natural frequencies match within acceptable limits for clamped–free and clamped–clamped conditions. However, for the simply supported condition the matching is not so good as in the other cases. The discrepancies may be due to the limitations of the experimental set not being able to provide truly clamped and pinned end supports. The disagreement is greater for the pinned ends case as the restraint against rotation at the ends was not completely eliminated by the fixtures.

3.1.3. *Variable section beams*

The proposed approach is used to obtain the natural frequencies and mode shapes for variable section cantilevered beams as chosen in the illustrative examples. Numerical results are generated with the following values of the beam parameters: $\rho = 2744$ kg/m^3, $E = 70{\cdot}0$ GPa, $L = 0{\cdot}60$ m, $b(0) = 0{\cdot}10$ m, $h(0) = 0{\cdot}00385$ m, $c(0)/\rho A(0) = 0{\cdot}56$ s^{-1}.

The boundary conditions of the beam are assumed as clamped at $s = 0$, and free at $s = L$. Two cases of variation of beam width and depth have been considered. These variations are chosen to represent a linear and non-linear convex (parabolic) taper. The width $b(s)$ at a distance s from the origin, can be written as

$$b(s) = b(0)[1 - w_1(s/L)] \text{ (linear)}, \qquad b(s) = h(0)[1 - w_1(s/L)^2] \text{ (parabolic)}, \tag{63}$$

in which $w_1 = 1 - b(L)/b(0)$. Similarly the thickness of the beam can be expressed by appropriately replacing $b(s)$ by $h(s)$, $b(0)$ by $h(0)$, $b(L)$ by $h(L)$ and w_1 by w_2 where $w_2 = 1 - h(L)/h(0)$.

The polynomial functions $f_1(s)$ and $f_2(s)$ for the stiffness, mass and damping variation along the span are expressed as

(i) *Linear*

$$\begin{aligned} f_1(s) &= 1 - (w_1 + 3w_2)(s/L) + 3(w_2^2 + w_1 w_2)(s/L)^2 \\ &\quad - (w_2^3 + 3w_1 w_2^2)(s/L)^3 + w_1 w_2^3 (s/L)^4, \\ f_2(s) &= 1 - (w_1 + w_2)(s/L) + w_1 w_2 (s/L)^2. \end{aligned} \tag{64}$$

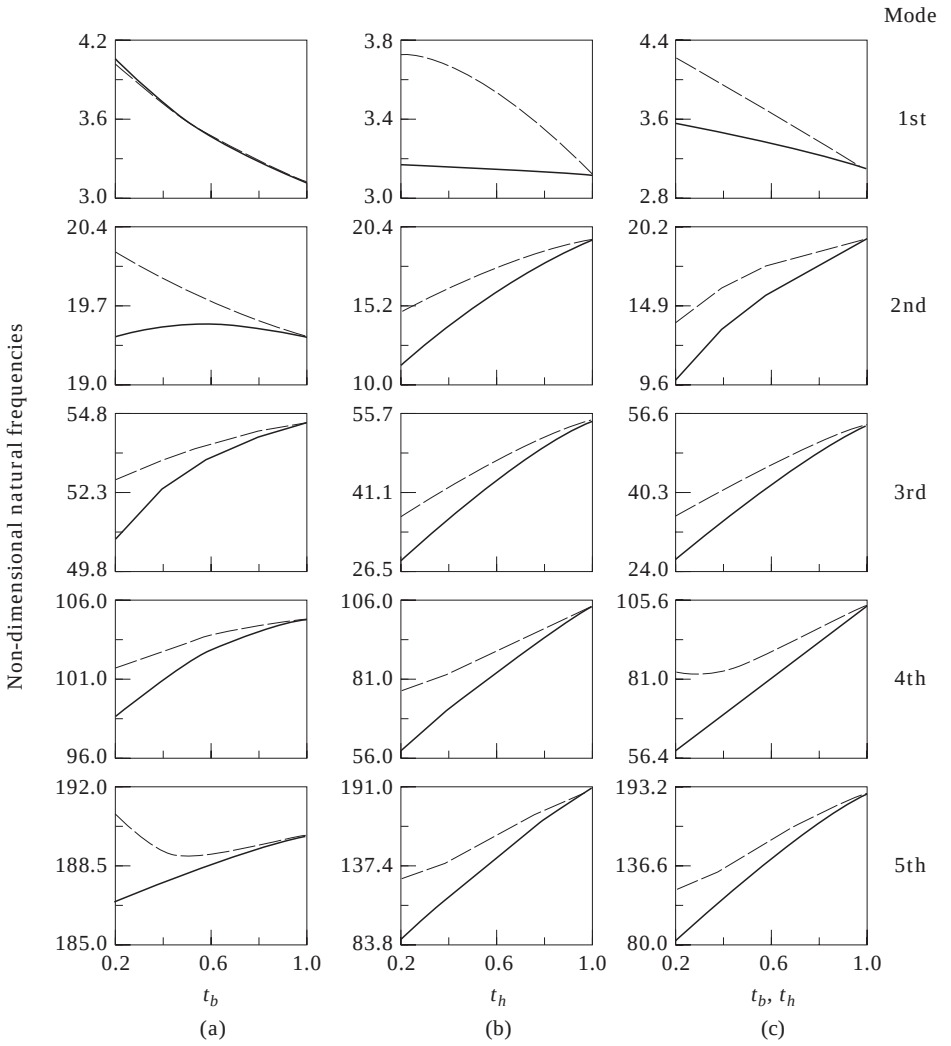

Figure 3. Effect of taper ratio on frequency number $(\Omega^2 m_0 l^4/EI_0)^{1/2}$. (a) width taper ($t_b = 1$); (b) height taper ($t_h = 1$); (c) width and height taper ($t_b = t_h$). Key: ——, Linear; ----, Parabolic.

(ii) *Parabolic*

$$f_1(s) = 1 - (w_1 + 3w_2)(s/L)^2 + 3(w_2^2 + w_1 w_2)(s/L)^4 - (w_2^3 + 3w_1 w_2^2)(s/L)^6 + w_1 w_2^3 (s/L)^8,$$

$$f_2(s) = 1 - (w_1 + w_2)(s/L)^2 + w_1 w_2 (s/L)^4. \tag{65}$$

The natural frequencies are obtained for the following forms of tapered cross-sections—width varying with thickness constant, thickness varying with width constant and width and thickness varying simultaneously. Loading is achieved by four concentrated masses M_1, M_2, M_3 and M_4 each equal to 0·0296 kg located at $0{\cdot}225L$, $0{\cdot}490L$, $0{\cdot}710L$ and $0{\cdot}980L$ respectively. With damping present, the eigenvalues α_i are complex and appear in conjugate pairs. The real part of α_i gives a decaying factor associated with each mode and magnitude of the imaginary part gives the corresponding damped natural frequency.

3.1.3.1. Effect of taper ratio on natural frequencies. Non-dimensional damped natural frequencies of a cantilevered beam in the first five modes for different combinations of taper are plotted against taper ratios and shown in Figure 3.

(a) *Width taper*, *height constant*

Figure 3(a) reveals the variation of the first five nodes with the two types of taper in width only. The fundamental frequency of the beam is seen to decrease with the increase

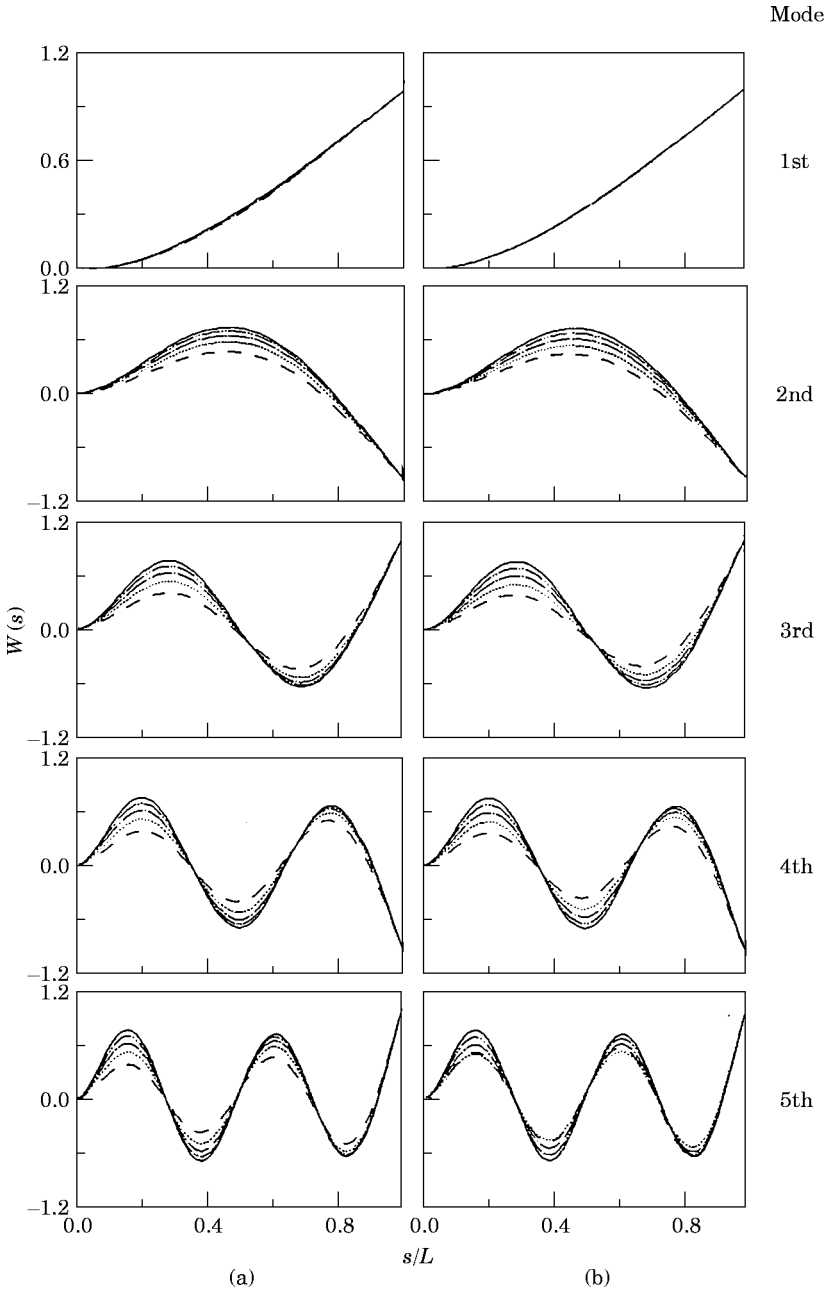

Figure 4. Effect of taper ratio on mode shape for (a) linear taper, (b) parabolic taper. Key: ----, $t_b = 0{\cdot}2$; . . . . . , $t_b = 0{\cdot}4$; —·—·—·—, $t_b = 0{\cdot}6$; —··—··—··—, $t_b = 0{\cdot}8$; ——, $t_b = 1{\cdot}0$.

in taper ratio for linear as well as parabolic shapes. At lower taper ratios, the parabolically tapered beam has slightly lower natural frequencies. In the second mode, for the parabolically tapered beam, the modal frequency gradually falls with the increase in taper ratio. The modal frequency of the linearly tapered beam shows low sensitivity to taper ratio with a small rise in value in the middle of the range considered. The third and fourth modal frequencies of the beam show increasing values with taper ratios for both linear and parabolically tapered beams. A similar pattern is observed for the linearly tapered beam in the fifth bending mode. Parabolically tapered beam, however, shows a different behaviour. The modal frequency is seen to decrease first and then increase with taper ratios, achieving a minimum value close to a taper ratio of 0·5. Except for the first mode, the natural frequency of the parabolically tapered beam is found to be higher in the first five modes considered.

(b) *Height taper*, *width constant*

The variation of the first five frequency numbers with taper in height and width constant is shown in Figure 3(b). In the case of the first mode, the fundamental frequency for the parabolic tapered beam decreases strongly with an increase in value of the taper ratio. However, the linearly tapered beam is almost insensitive to taper ratio, showing a very small decrease with increased taper ratio. Second, third, fourth and fifth modal frequencies are seen to increase with an increase in taper ratio. The natural frequency for the parabolic tapered beam is seem to be higher than the linearly tapered beam for all the modes considered.

(c) *Height and width taper*

The variation of modal frequencies when both width and height taper simultaneously in the same proportion, are presented in Figure 3(c). The first modal frequency is seen to decrease with an increase in taper ratio for both types of beams showing non-linear trends. The second, third, fourth and fifth modal frequencies are seen to increase with taper ratios. This is observed for both linear and parabolically tapered beams.

3.1.3.2. Effect of taper ratio on mode shape. The shape function $W(s)$ for different values of tapered ratios for a cantilevered beam are shown in Figure 4. To avoid an excessive number of graphs, only the width taper has been considered to illustrate the displaced configuration of the beam in its natural modes. Five taper ratios ($t_b = 0{\cdot}2$, $0{\cdot}4$, $0{\cdot}6$, $0{\cdot}8$, $1{\cdot}0$) have been considered with linear and parabolic taper shapes. Mode shapes are normalized with absolute value of corresponding tip deflections. Figure 4(a) shows the mode shape with a linearly tapered width while Figure 4(b) presents results for the parabolically tapered shape. The clamped end is always a nodal point for the cantilever beam. In the first mode, no significant change is observed for the displacement pattern with change in taper ratio. As taper ratio increases the nodal point has a tendency to shift towards the free tip and maximum displacement in the mode shape increases for all the modes studied. The shift in the node point location becomes less prominent with increased modal number. The basic behaviour of the displacement function for the parabolic beam seems to follow the same pattern as the linearly tapered beam. The shift in the node point is greater for the parabolically tapered beams.

3.1.3.3. Effect of mass location on natural frequency. The effect of location of a single concentrated mass ($M_1 = 0{\cdot}1184$ kg) on the non-dimensional natural frequency number of the tapered beam is shown in Figure 5 for different combinations of taper. Only one value of the taper ratio is considered to illustrate the results.

In Figure 5(a), the first five modal frequencies of the beam tapered in width only are shown for linearly and parabolically tapered beams with taper ratio $t_b = 0{\cdot}4$. In the first mode, for both types of taper, the frequency increases as the point mass moves from tip towards the support. In the second, third, fourth and fifth modes, frequency shows a strong

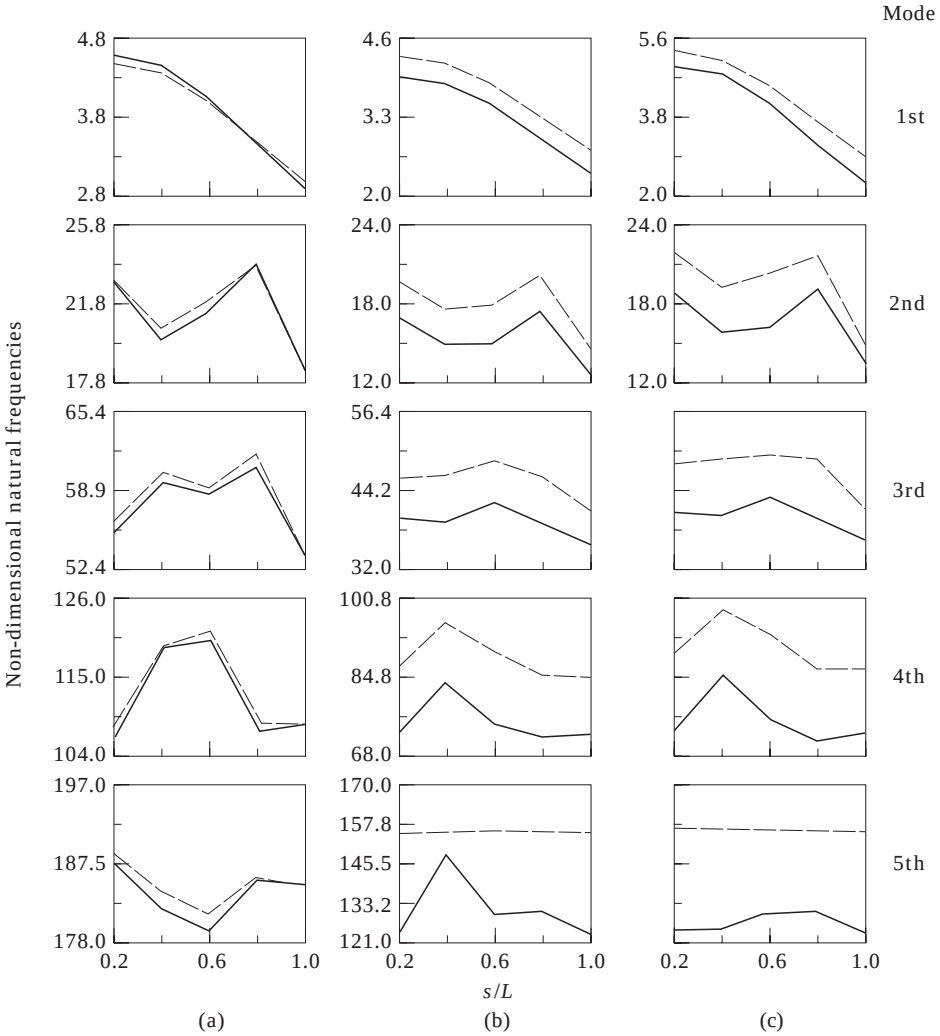

Figure 5. Effect of mass location on frequency number $(\Omega^2 m_0 l^4/EI_0)^{1/2}$ for (a) width taper ($t_h = 1$); (b) height taper ($t_b = 1$); (c) width and height taper ($t_b = t_h$). Key: as for Figure 3.

dependence on the position of mass, but no regular pattern can be observed. Both types of taper in general show a similarity in frequency behaviour. In the first mode, the natural frequency of the parabolically tapered beam is higher than of the linearly tapered beam when the mass is near the tip and is lower with the mass closer to the root. In all other cases, for most of the location of concentrated mass, the natural frequency of parabolically tapered beam seems to be higher than for the linearly tapered beam.

Figure 5(b) presents the variation of frequency numbers for the beam tapered in height only with width constant. The first mode frequency decreases as the mass travels towards the tip. Second, third, fourth and fifth mode frequency numbers in linearly tapered beams do not reveal any regular pattern of variation. The parabolically tapered beam follows a similar pattern in all the higher modes except in the fifth mode. In the fifth mode, the modal frequency of the parabolically tapered beam decreases only marginally as the mass is

moved towards the tip. For every location of concentrated mass, the parabolically tapered beam shows a higher value of natural frequency in the first five modes considered.

The simultaneous variation of modal frequency of the beam with identical width and height taper is shown in Figure 5(c) for various locations of a single concentrated mass. Linear as well as parabolically tapered beams show decreasing values of the fundamental frequency with the shifting of the mass towards the free end. Second, third, fourth and fifth frequency numbers do not show any predictable pattern of variation with the location of the mass for the linearly tapered beam. Parabolically tapered beam shows more or less similar behaviour in the second, third and fourth modes. However, in the fifth mode, no significant change in frequency with the change in location of the mass can be observed.

3.2. RESPONSE STATISTICS

The response-time history of the first three normal co-ordinates of a cantilever beam are shown in Figures 6 and 7. The curves are plotted with three different values of taper ratios, $t_b = 0{\cdot}2$, $0{\cdot}4$, $0{\cdot}6$ and $t_h = 1$. The input characteristics are $z_0 = 0{\cdot}05$ m, $\omega_0 = 1{\cdot}25$ rad/s, $\sigma = 0{\cdot}015$ m, $\beta_1 = 8{\cdot}0$.

3.2.1. *Mean response*

Figure 6 presents the mean response of the first three normal co-ordinates for a linearly tapered cantilever beam. The steady state pattern of response under sinusoidal mean input is reflected in displacement, velocity and acceleration time histories. Mean displacement at the start of the motion is higher than the steady state value. Mean velocity shows that amplitude builds up gradually to attain a steady state pattern of oscillation. Response with different values of taper ratio shows that magnitude increases with an increase in taper ratio. This is expected as with an increase in taper ratio, the dynamic stiffness of the beam decreases.

The mean response of the second normal co-ordinate is seen to follow the same pattern as the first mode. However, it has significantly lower magnitude than the first mode

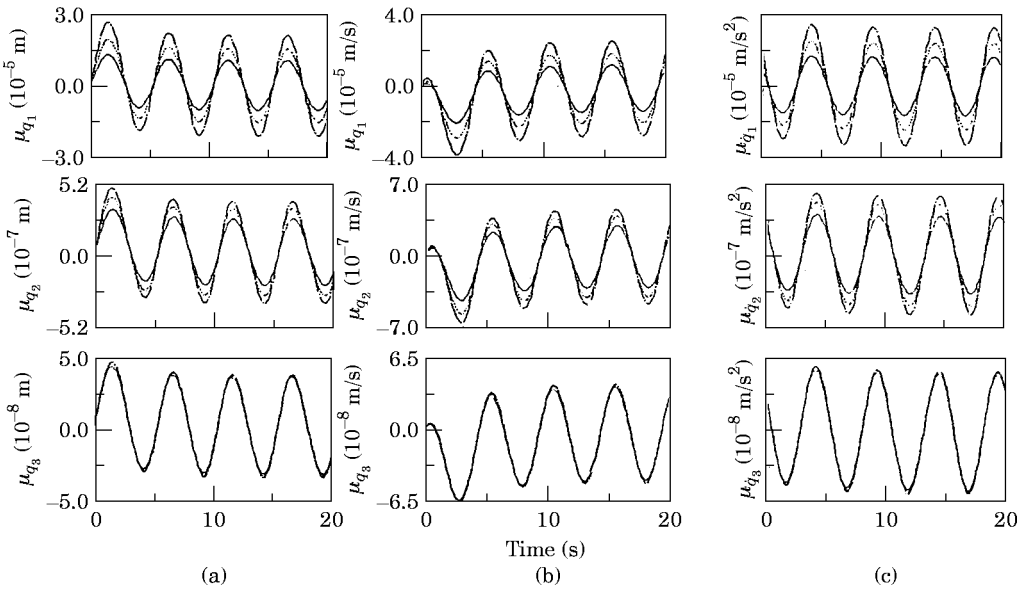

Figure 6. Mean response of a linearly tapered beam for (a) displacement, (b) velocity, (c) acceleration. Key: ——, $t_b = 0{\cdot}2$; . . . . . , $t_b = 0{\cdot}4$; —·—·—, $t_b = 0$.

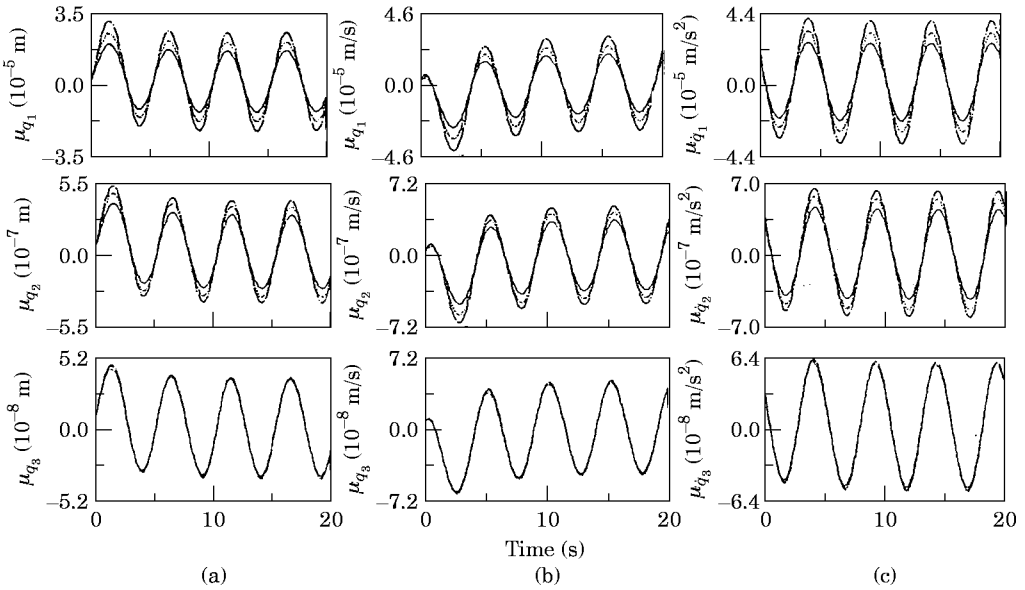

Figure 7. Mean response parabolically tapered beam for (a) displacement, (b) velocity, (c) acceleration. Key: as for Figure 6.

response. The mean displacement, velocity and acceleration of the third normal co-ordinate has a similar pattern as the first and second modes. The response magnitude is lower in comparison to the second mode. However, the response shows little change in magnitude with change in the taper ratios.

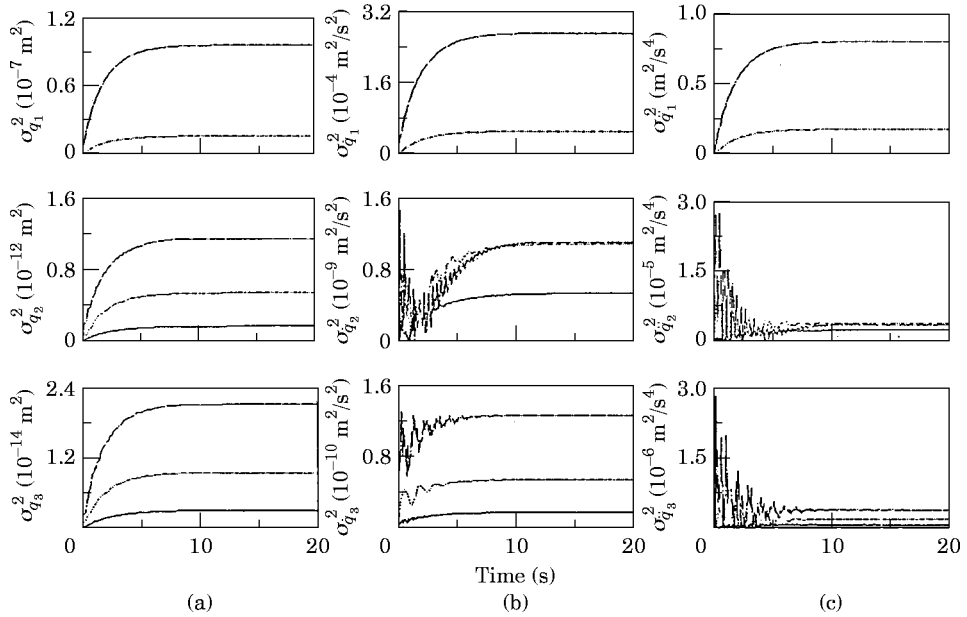

Figure 8. Response variance of a linearly tapered beam for (a) displacement, (b) velocity, (c) acceleration. Key: as for Figure 6.

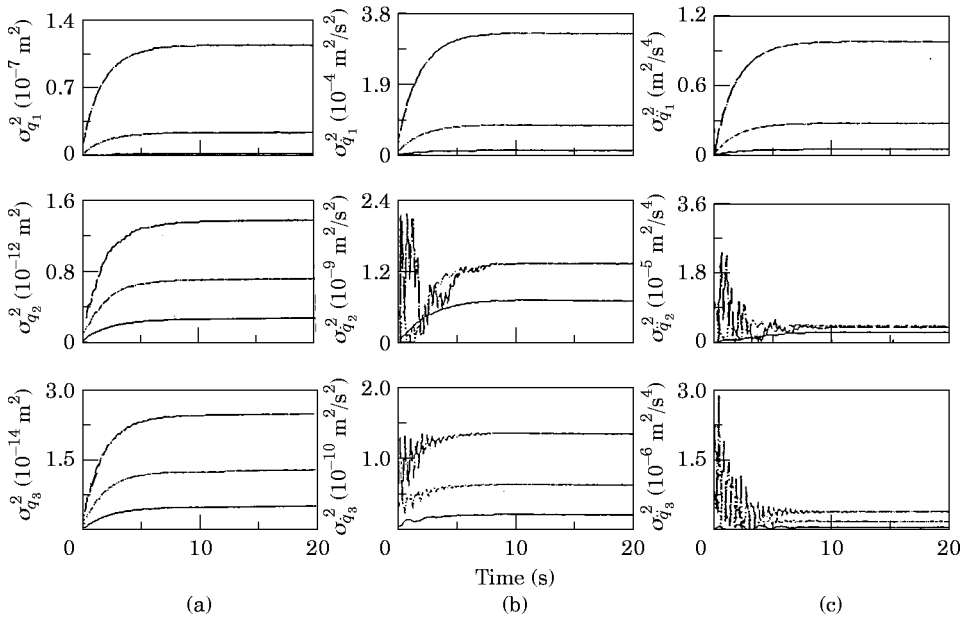

Figure 9. Response variance of a parabolically tapered beam for (a) displacement, (b) velocity, (c) acceleration. Key: as for Figure 6.

The mean response of the parabolically tapered beam is shown in Figure 7 for its first three normal co-ordinates. The behaviour is found to be similar to that of the linearly tapered beam. First and second mode response magnitudes are seen to be higher in comparison to the linearly tapered beam. However, no significant change in response magnitude can be observed in the two beams for the third normal co-ordinates.

3.2.2. *Response variance*

Variance of response quantities for the linearly tapered beam is presented in Figure 8, and that for the parabolically tapered beam in Figure 9.

Displacement, velocity and acceleration variances of the first normal co-ordinate for the linearly tapered beam shows that the response rises to attain a steady value. The steady state value is much higher for the beam with a higher value of taper ratios.

For the second normal co-ordinate, displacement variance for the beam with higher taper ratio fluctuates in the early stage. These fluctuations die out to attain an asymptotic value. Displacement variance is found to be higher for higher taper ratios. For the second normal co-ordinate, the variance of velocity indicates a different pattern. Fluctuations are observed in the early period for all the taper ratios considered. Fluctuations are more prominent in the case of higher taper ratios. The magnitude is seen to increase with taper ratio but the difference becomes small in the two higher taper ratios used. Acceleration variance in the second mode shows an initial high value with strong fluctuations which decreases to attain a low level of steady state value.

Variance of displacement, velocity and acceleration response in the third normal co-ordinate follow the trend similar to the second. Beams with higher taper ratios are seen to have a higher response variance. The magnitude of the variance decreases with the increase in the normal co-ordinate mode number.

Response variances of the parabolically tapered beam for the first three normal co-ordinates are shown in Figure 9. The behaviour, in general, is found to be similar to

that of the linearly tapered beam. The magnitudes are marginally higher compared to the corresponding linear taper beam response.

A comparison of mean and variance for all the normal co-ordinates shows that the first mode response is considerably higher than that of the higher modes. This indicates that inclusion of only the first few modes in the response calculation is appropriate.

4. CONCLUSIONS

An analytical approach has been outlined to study the free and forced vibrational characteristics of a non-uniform beam carrying several concentrated masses. Stationary as well as non-stationary random input can be handled by the approach. The beam mass and stiffness variations can be of a general nature with damping proportional to mass distribution. The approach is applicable to any type of boundary conditions. Comparison with experimental results and data available in the literature validates the present approach. The approach is illustrated with a cantilever beam with support excitation. Some conclusions drawn from the study are

(1) The natural frequency of the non-uniform beam is sensitive to change in the taper ratio and magnitude and location of the concentrated mass loading present in the beam.

(2) Forced response is found to be influenced not only by the input characteristics but also by the change in the beam profile.

(3) The polynomial mode shape function derived will be of much help in the analysis of non-uniform flexible structures modelled by finite beam elements. The use of the non-uniform beam shape functions instead of the traditional uniform beam functions in the finite element analysis is expected to produce rapid convergence with a smaller number of elements.

REFERENCES

1. H. D. Conway and J. F. Dubil 1965 *Transactions of the American Society of Mechanical Engineers*, *Journal of Applied Mechanics* **32**, 932–935. Vibrational frequencies of truncated cone and wedge beams.
2. D. J. Sanger 1968 *Journal of Mechanical Engineering Science* **16**, 111–120. Transverse vibration of a class of nonuniform beam.
3. D. J. Gorman 1975 *Free Vibrational Analysis of Beams and Shafts*. John Wiley.
4. R. P. Goel 1976 *Journal of Sound and Vibration* **47**, 1–7. Transverse vibration of tapered beams.
5. H. C. Wang 1967 *Transactions of the American Society of Mechanical Engineers*, *Journal of Applied Mechanics* **34**, 702–708. Generalised hypergeometric function solution on the transverse vibration of a class of nonuniform beam.
6. S. Naguleswaran 1992 *Journal of Sound and Vibration* **153**, 509–532. Vibration of an Euler–Bernoulli beam of constant depth and with linearly varying breadth.
7. S. Naguleswaran 1994 *Journal of Sound and Vibration* **172**, 289–304. A direct solution for the transverse vibration of Euler–Bernoulli wedge and cone beams.
8. S. Abrate 1995 *Journal of Sound and Vibration* **185**, 703–716. Vibration of non-uniform rods and beams.
9. Y. Chen 1963 *Transactions of the American Society of Mechanical Engineers*, *Journal of Applied Mechanics* **30**, 310–311. On the vibration of beams and rods carrying a concentrated mass.
10. W. E. Baker 1964 *Transactions of the American Society of Mechanical Engineers*, *Journal of Applied Mechanics* **31**, 335–337. Vibration frequencies of uniform beams with central mass.
11. P. A. A. Laura, J. L. Pombo and E. A. Susemihl 1974 *Journal of Sound and Vibration* **37**, 161–168. A note on the vibration of a clamped free beam with a mass at the free end.
12. P. A. A. Laura, M. J. Maurizi and J. L. Pombo 1975 *Journal of Sound and Vibration* **41**, 397–405. A note on the dynamic analysis of an elastically restrained free beam with a mass at the free end.

13. C. N. Bapat and C. Bapat 1987 *Journal of Sound and Vibration* **112**, 177–182. Natural frequencies of a beam with non-classical boundary conditions and concentrated masses.
14. H. H. Mabie and C. B. Rogers 1972 *Journal of the Acoustical Society of America* **51**, 1771–1774. Transverse vibration of a double tapered cantilever beam.
15. D. S. Chehil and R. Jategaonkar 1987 *Journal of Sound and Vibration* **115**, 423–436. Determination of natural frequencies of a beam with varying section properties.
16. C. S. Kim, S. M. Dickinson 1988 *Journal of Sound and Vibration* **122**, 441–455. On the analysis of laterally vibrating beams subject to various complicating effects.
17. C. W. S. To 1981 *Journal of Sound and Vibration* **78**, 475–484. A linearly tapered beam finite element incorporating shear and rotary inertia for vibration analysis.
18. D. E. Beskos 1987 *Applied Mechanics Review* **40**, 1–23. Boundary element method in dynamic analysis.
19. R. H. Guitierrez and P. A. A. Laura 1994 *Ocean Engineering* **21**, 57–66. The method of differential quadrature and its application to the approximate solution of ocean engineering problems.
20. C. W. S. To 1982 *Journal of Sound and Vibration* **83**, 445–460. Vibration of cantilever beam with base excitation and tip mass.
21. H. K. Milne 1989 *Journal of Sound and Vibration* **131**, 353–365. The receptance function of uniform beams.
22. D. N. Manikanhally and M. J. Crocker 1989 *Journal of Sound and Vibration* **132**, 177–197. Vibration analysis of hysteritically damped mass loaded beam.
23. P. A. A. Laura and B. Valerga de Greco 1988 *Journal of Sound and Vibration* **120**, 587–597. Numerical experiments on free and forced vibrations of beams of non-uniform cross section.
24. S. Y. Lee, H. Y. Ke and Y. H. Kuo 1990 *Journal of Sound and Vibration* **142**, 15–29. Analysis of non-uniform beam vibration.
25. A. C. Eringen 1957 *Transactions of the American Society of Mechanical Engineers*, *Journal of Applied Mechanics* **24**, 46–52. Response of beams and plates to random loads.
26. J. C. Samuels and A. C. Eringen 1958 *Transactions of the American Society of Mechanical Engineers*, *Journal of Applied Mechanics* **25**, 496–500. Response of a simply supported Timoshenko beam to a purely random Gaussian process.
27. S. H. Crandall and A. Yildiz 1962 *Transactions of the American Society of Mechanical Engineers*, *Journal of Applied Mechanics* **29**, 267–275. Random vibration of beams.
28. J. Cederkvist 1982 *Journal of Structural Mechanics* **10**, 49–65. Design of beams subject to random loads.
29. G. Ahmadi and M. A. Satter 1975 *American Institute of Aeronautics and Astronautics Journal* **13**, 1097–1100. Mean square response of beams to nonstationary random loads.
30. C. W. S. To 1982 *Journal of Sound and Vibration* **83**, 273–291. Non-stationary random response of a multi-degree-of-freedom-system by the theory of evolutionary spectra.
31. R. W. Clough and J. Penzien 1993 *Dynamics of Structures*. New York: McGraw Hill.
32. D. Yadav and H. C. Upadhyay 1991 *Journal of Sound and Vibration* **147**, 57–71. Non-stationary dynamics of train and flexible track over inertial foundation during variable velocity run.
33. I. S. Gradshteyn and I. M. Ryzhik 1980 *Tables of Integral*, *Series and Products*. New York: Academic Press.
34. N. C. Nigam 1983 *Introduction to Random Vibration*. Cambridge, MA: MIT Press.